EPJ A direct
electronic only

Study of the ^{106}Cd$(\alpha, \alpha)^{106}$Cd scattering at energies relevant to the p-process

G.G. Kiss[1,2,a], Zs. Fülöp[1], Gy. Gyürky[1], Z. Máté[1], E. Somorjai[1], D. Galaviz[3,b], A. Kretschmer[3], K. Sonnabend[3], and A. Zilges[3]

[1] Institute of Nuclear Research (ATOMKI), P.O. Box 51, H-4001 Debrecen, Hungary
[2] University of Debrecen, Debrecen, Hungary
[3] Technische Universität Darmstadt, D-64289 Darmstadt, Germany

Abstract. The elastic scattering cross section of ^{106}Cd$(\alpha, \alpha)^{106}$Cd has been measured with high accuracy at energies of $E_{c.m.} \approx 15.5$, 17, and 19 MeV. The optical potential for the system ^{106}Cd $\otimes \alpha$ has been derived at energies above and below the Coulomb barrier. Predictions for the ^{106}Cd$(\alpha, \gamma)^{110}$Sn capture cross section at astrophysically relevant energies are presented and compared to the experimental data measured recently.

PACS. 24.10.Ht Optical and diffraction models – 25.55.-e ^{3}H-, ^{3}He-, and ^{4}He-induced reactions – 25.55.Ci Elastic and inelastic scattering – 26.30.+k Nucleosynthesis in novae, supernovae and other explosive environments

1 Introduction

The nucleosynthesis of nuclei above the iron peak proceeds mainly by neutron capture in the s- and r-process. However, there are 35 other, stable, proton-rich, the so-called p-nuclei, which cannot be produced via neutron capture reactions [1]. The production of the p-nuclei proceeds mainly via photon-induced reactions in the O/Ne layers of type-II supernovae. The s and r seed nuclei are disintegrated by (γ, n), (γ, p) and (γ, α) reactions in the high photon flux of the explosion.

Calculations for the p-process involve more than 1000 nuclei in a network that requires more than 10000 reaction rates [2]. Almost none of these reaction rates has been measured and the calculations rely completely on the statistical model. One of the input parameters in statistical model calculations to determine (γ, α) reaction rates is the alpha-nucleus optical potentials. However, the uncertainties shown by the alpha-nucleus potentials at astrophysically relevant energies are large [3,4]. Experimental informations are therefore required to reduce the uncertainties in the calculation of (γ, α) reaction rates.

In principle, the alpha-nucleus potentials can be determined from alpha elastic scattering experiments. The fea-

sibility of such a measurement is, however, limited in general because the experimentally determined cross section at energies below the Coulomb barrier shows only a small deviation from the Rutherford cross section and the results have ambiguities. In recent years, however, alpha-nucleus potential parameters of ^{144}Sm, ^{92}Mo, ^{112,114}Sn have been successfully derived at ATOMKI [4,5,6]. A new experiment on ^{106}Cd, the most proton-rich stable isotope of Cd, helps to better understand the behavior of the alpha-nucleus optical potential as a function of the mass number and energy.

The choice of the measured energies at about 15.5, 17 and 19 MeV has the following reason. The Gamow-window for (γ, α) reactions at $T_9 \approx 2$–3 is in the range of $E_\gamma \approx 5$–10 MeV corresponding to 4–9 MeV for the inverse ^{106}Cd$(\alpha, \gamma)^{110}$Sn reaction. Recently the (α, γ) capture cross section on ^{106}Cd has been measured in the upper part and above the Gamow-window [7,8]. The experimental determination of the nuclear part of the optical potential at this astrophysical energy, however, is impossible, because of the dominating Coulomb interaction. The height of the Coulomb barrier is about 18.2 MeV. The aim of the present work is to determine the optical potential at the lowest possible energies, moreover, at several energies above and below the Coulomb barrier to be able to extrapolate the optical potential parameters to the astrophysically relevant energy region. We finally compare the measured (α, γ) cross section of ^{106}Cd with the pre-
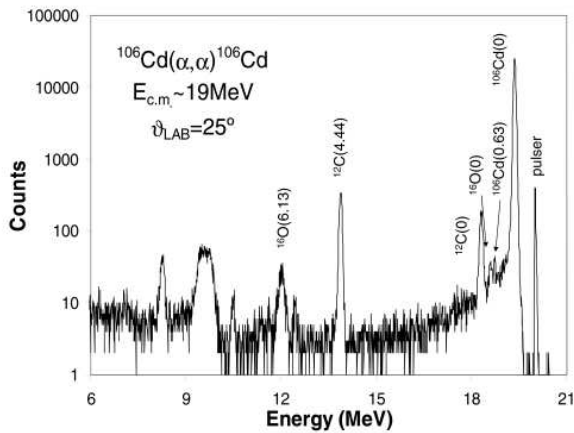
Fig. 1. Typical spectrum of ^{106}Cd$(\alpha,\alpha)^{106}$Cd at $\vartheta = 25°$. Elastic scattering on target contaminations (mainly ^{12}C from the carbon backing) and inelastically scattered particles are clearly separated from the elastic peak. The pulser peak used for the dead time correction is also shown.

Fig. 2. Relative yield of ^{12}C recoil nuclei in coincidence with elastically scattered alpha-particles. The gray area presents the angle and the uncertainties expected from the reaction kinematics. A Gaussian fit to the experimental data (solid line) is shown to guide the eye.

dictions of statistical model calculations using the optical potential parameters derived in this work.

2 Experimental setup and procedure

The scattering experiment was performed at the cyclotron laboratory at ATOMKI, Debrecen. Complete angular distributions between 20° and 170° were measured in steps of 1° ($20° \leq \vartheta \leq 100°$), 1.5° ($100° \leq \vartheta \leq 140°$) and 2° ($140° \leq \vartheta \leq 170°$) at alpha energies of $E_{Lab} = 16.13$ MeV, 17.65 MeV and 19.61 MeV. The beam intensity was 150 pnA. A typical spectrum of ^{106}Cd$(\alpha,\alpha)^{106}$Cd reaction is shown in fig. 1.

The highly enriched ($\approx 97\%$) cadmium targets were produced by evaporation at the target laboratory at ATOMKI. A thin carbon foil ($\approx 20\,\mu$g/cm^2) was used as backing. The thickness of the target was roughly $250\,\mu$g/cm^2. The target was mounted on a remotely controlled target ladder in the centre of the scattering chamber. The stability of the target was monitored during the whole experiment to avoid systematic uncertainties from changes in the target.

An aperture of 2×6 mm was mounted on the target holder to check the beam position and size of the beam spot before and after every change of beam energy or current. We optimized the beam until not more than 1% of the total beam current could be measured on this aperture. As a result, the horizontal size of the beam spot was smaller than 2 mm during the whole experiment which is very important for the precise determination of the scattering angle.

Taking into account the Q values of the open reaction channels, particle ID was not necessary. For the measurement of the angular distribution we used four surface barrier detectors with an active area of 50 mm^2. The detectors were mounted on upper and lower turntables, the angular distance between two detectors on the same

turntable was 10°. The solid angles of the detector pairs were $\Delta\Omega = 1.63 \times 10^{-4}$ and $\Delta\Omega = 1.55 \times 10^{-4}$. The ratios of the solid angles of the different detectors were checked by measurements at overlapping angles with an accuracy of better than 1%.

Additionally, two detectors were mounted at the wall of the scattering chamber at a fixed angle of $\vartheta = \pm 15°$ with respect to the beam direction. These detectors were used as monitor detectors during the experiment to normalize the measured angular distribution and to determine the precise position of the beam spot. The solid angle of these detectors was $\Delta\Omega = 8.1 \times 10^{-6}$.

The signals from the detectors were amplified using charge-sensitive preamplifiers, which were mounted directly at the scattering chamber. The output signal was led to the main amplifier and fed into an analog-digital converter. For the coincidence measurements (see below) the bipolar signals of the main amplifiers were fed into timing single-channel analyzers, and the unipolar outputs were gated using linear gate stretchers.

The angular calibration of the setup is of crucial importance for the precision of the scattering experiments at energies close to the Coulomb barrier because the Rutherford cross section depends very sensitively on the angle. Small uncertainties of 0.1° in the determination of the scattering angle lead to uncertainties of 2% in the cross section at forward angles. To determine the scattering angle precisely, we measured kinematic coincidences between elastically scattered alpha-particles and the corresponding ^{12}C recoil nuclei using a pure Carbon foil as target. One detector was placed at $\vartheta = 80°$ and the signals from the elastically scattered alpha particles on ^{12}C were selected as gates for signals from another detector which moved around the expected ^{12}C recoil angle $\vartheta = 40.2°$, fig. 2. shows the relative yield of ^{12}C recoil nuclei in coincidence with elastically scattered alpha particles as a function of the ^{12}C recoil angle. In this way the final angular uncertainties of our setup was determined to be 0.07°.

Table 1. Parameters of the real and imaginary part of the alpha-nucleus optical potential of ^{106}Cd.

a^*(MeV fm^3)	b^*(fm^3)	$J_{R,0}$	ω	W_V(MeV)	R_V(fm)	a_V(fm)	W_S(MeV)	R_S(fm)	a_S(fm)
377.99	-0.6519	266.91	0.987	-2.879	1.744	0.347	339.01	1.262	0.206
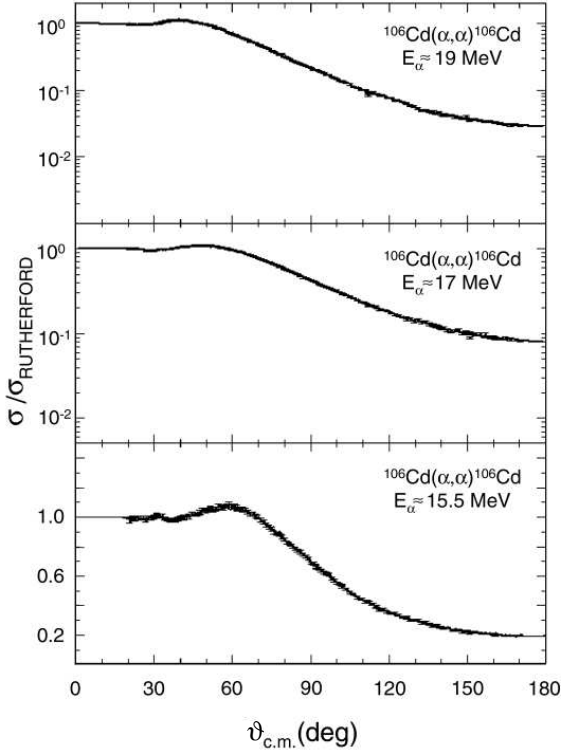
Fig. 3. Experimental cross section of ^{106}Cd(α, α)^{106}Cd at $E_{c.m.} \approx 19$, 17 and 15.5 MeV normalized to the Rutherford cross section.

The count rates $N(\vartheta)$ in the four detectors have been normalized to the number of counts in the monitor detectors $N_{MON.}(\vartheta = 15°)$:

$$\left(\frac{d\sigma}{d\Omega}\right)(\vartheta) = \left(\frac{d\sigma}{d\Omega}\right)_{MON.} \frac{N(\vartheta)}{N_{MON.}} \frac{\Delta\Omega_{MON.}}{\Delta\Omega}, \qquad (1)$$

where $\Delta\Omega$ is the solid angle of the detector. The cross section at the monitor detectors is given by the Rutherford cross section owing to the low scattering angle. The beam was stopped in a Faraday cup and the beam current was measured by a current integrator.

The absolute cross sections cover five orders of magnitude in the measured angular range. However the statistical uncertainties of each data point changes only from $\leq 0.3\%$ (forward angles) to about 1%–2% (backward angles). The experimental cross section normalized to the Rutherford cross section is shown in fig. 3.

3 Optical potential parameters

In order to determine the alpha nucleus potential of ^{106}Cd, we have performed our analysis in the framework of the

Optical Model (OM). The optical potential takes the form

$$U(r) = V_C(r) + V(r) + iW(r), \qquad (2)$$

where $V_C(r)$ is the Coulomb potential, $V(r)$ and $W(r)$ are the real and imaginary parts of the nuclear potential, respectively. The description of $V(r)$ is done using the double-folding procedure, in which both nuclei interact via an effective nucleon-nucleon interaction in the well-established DDM3Y parametrization [9,10]. The real part of the nuclear potential is based on this double-folding potential $V_f(r)$, in which two small corrections in strength (λ) and width ($\omega \approx 1.0$) have been applied:

$$V(r) = \lambda V_f(r/\omega). \qquad (3)$$

The parameter ω is introduced to modify the width of the potential. Through this rearrangement, it is possible to correct the deviations between the proton and neutron density distributions within the nucleus. For stable light nuclei with $Z = N$ there is no need for such a parameter. In case of medium or heavy nuclei with a neutron-to-proton ratio of $N/Z \geq 1.2$ it is necessary to take this correction into consideration.

The strength parameter λ has been described by a linear form:

$$\lambda = \frac{a^* + b^* E_{c.m.}}{J_{R,0}}. \qquad (4)$$

The coefficients a^* and b^* are listed in table 1. The volume integral of the potential $J_{R,0}$ for $\lambda = 1.0$ and the corresponding ω are also listed. The weak energy dependence of the volume integral through b^* reduces the uncertainties of the extrapolation to the astrophysically relevant energy region.

For a comparison of different potentials we use the integral parameters such as the volume integral per interacting nucleon pair J_R and the root-mean-square (rms) radius $r_{rms,R}$, which are given by

$$J_R = \frac{1}{A_p A_T} \int V(r) \, d^3r, \qquad (5)$$

$$r_{rms,R} = \sqrt{\frac{\int V(r) r^2 \, d^3r}{\int V(r) \, d^3r}}, \qquad (6)$$

for the real part of the potential $V(r)$ and the corresponding equations hold for $W(r)$. The Coulomb potential is taken in the usual form of a homogeneously charged sphere. In the imaginary part of the nuclear potential we have tested different parameterizations. It turned out that the best fit to our experimental data is given by the combination of volume (V) and surface (S) Wood-Saxons potentials. The relative weight between the volume and surface
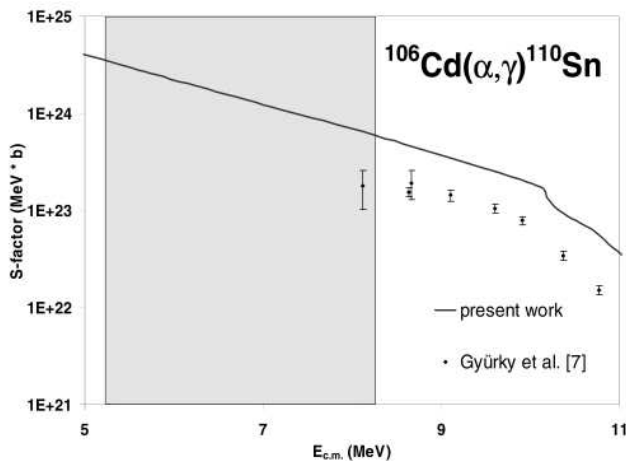
Fig. 4. Astrophysical S-factor of ^{106}Cd$(\alpha,\gamma)^{110}$Sn capture reaction. The experimental data from [7,8] are compared to the optical potential obtained from the analysis of the scattering data. The gray area shows the energy region relevant to the p-process.

terms of the imaginary part of the nuclear potential is $J_{I,V} = 0.22 J_{I,S}$, as found in a study of the elastic scattering data in the $A \approx 100$ mass region [11]. This dominance of the surface Woods-Saxon term at energies close to the Coulomb barrier provides a better description of the alpha capture data at the astrophysically interesting energy window. The calculations were performed using the A0 code [12]. The resulting best fit parameters are shown in table reftab:1. For details of the fitting procedure see [13].

Due to the astrophysical interest, the laboratory (α,γ) reaction cross section on ^{106}Cd nucleus has been measured close to the Gamow-window [7,8]. The preliminary astrophysical S-factor of the reaction ^{106}Cd$(\alpha,\gamma)^{110}$Sn is shown in fig. 4. In addition, the predictions from statistical model calculations using alpha-nucleus optical potential derived in this work are as input parameters for the NON-SMOKER code [14] are plotted as well.

It is also instructive to compare the results of the present experiment with the calculated scattering cross sections using different global alpha-nucleus potentials.

This work is still in progress and it is beyond the scope of the present paper.

References

1. M. Arnould, S. Goriely, Phys. Rep. **384**, 1 (2003).
2. T. Rauscher, A. Heger, R.D. Hoffman, S.E. Woosley, Astrophys. J. **576**, 323 (2002).
3. E. Somorjai, Zs. Fülöp, A.Z. Kiss, C.E. Rolfs, H.-P. Trautvetter, U. Greife, M. Junker, S. Goriely, M. Arnould, M. Rayet, T. Rauscher, H. Oberhummer, Astron. Astrophys. **333**, 1112 (1998).
4. P. Mohr, T. Rauscher, H. Oberhummer, Z. Máté, Zs. Fülöp, E. Somorjai, M. Jaeger, G. Staudt, Phys. Rev. C **55**, 1523 (1997).
5. Zs. Fülöp, Gy. Gyürky, E. Somorjai, L. Zolnai, D. Galaviz, M. Babilon, P. Mohr, A. Zilges, T. Rauscher, H. Oberhummer, Phys. Rev. C **64**, 065805 (2001).
6. D. Galaviz, Zs. Fülöp, Gy. Gyürky, Z. Máté, P. Mohr, T. Rauscher, E. Somorjai, A. Zilges, Phys. Rev. C **71**, 065802 (2005).
7. Gy. Gyürky, Zs. Fülöp, G.G. Kiss, Z. Máté, E. Somorjai, J. Görres, A. Palumbo, M. Wiescher, D. Galaviz, A. Kretschmer, K. Sonnabend, A. Zilges, T. Rauscher Nucl. Phys. A **758**, 517c (2005).
8. Gy. Gyürky, Z. Elekes, Zs. Fülöp, G.G. Kiss, E. Somorjai, J. Görres, A. Palumbo, M. Wiescher, W. Rapp, N. Özkan, R.T. Gürray, T. Rauscher, in preparation.
9. G.R. Satchler, W.G. Love, Phys. Rep. **55**, 183 (1979).
10. A.M. Kobos, B.A. Brown, R. Lindsay, G.R. Satchler, Nucl. Phys. A **425**, 205 (1984).
11. T. Rauscher, in *Proceedings of the IX Workshop on Nuclear Astrophysics* (1998).
12. H. Abele, University of Tübingen, computer code A0, unpublished.
13. D. Galaviz, PhD Thesis, TU Darmstadt (2004).
14. T. Rauscher, F.K. Thielemann, At. Data Nucl. Data Tables **79**, 47 (2001).